Opt Quant Electron (2014) 46:581–591
DOI 10.1007/s11082-013-9849-z

Performance limits of the mid-wave InAsSb/AlAsSb nBn HOT infrared detector

P. Martyniuk · A. Rogalski

Received: 22 April 2013 / Accepted: 25 November 2013 / Published online: 19 December 2013

Abstract InAsSb ternary alloy is considered to be an alternative to HgCdTe (MCT) in mid-wavelength infrared spectral region. The high operation temperature conditions are successfully reached with $A^{III}B^{V}$ bariodes, where InAsSb/AlAsSb system is playing dominant role. Since there is no depletion region in the active layer, the generation-recombination and trap-assisted tunneling mechanisms are suppressed leading to lower dark currents in comparison with standard photodiodes. As a consequence, the bariodes operate at a higher temperature than standard photodiodes which could be used in wide range of system applications, especially where the size, weight, and power consumption are crucial. The paper presents detailed analysis of the bariode's performance (such as dark and photocurrent, differential resistance area product, and detectivity) versus applied voltage, operating temperatures and structural parameters. The optimal working conditions are calculated. The theoretical predictions of bariode's performance are compared with experimental data published in the literature. Finally, the nBn InAsSb/AlAsSb performance is compared to the MCT "Rule 07".

Keywords InAsSb/AlAsSb nBn detector · Bariode · BIRD

1 Introduction

Photodetectors optimized for the mid-wavelength infrared (MWIR) spectral range and high operation temperature (HOT) conditions are in demand for variety of IR systems where the size, weight, and power (SWaP) consumption are important. The low dark current and high quantum efficiency (*QE*) are the key factors which must be met to design the HOT IR detector. In standard photodiodes operating under HOT conditions, the dark current is predominantly produced by the Shockley-Read-Hall (SRH) generation recombination process (GR), Auger GR and tunneling mechanism (Rogalski 2011; Martyniuk and Rogalski 2013a). The SRH

P. Martyniuk (✉) · A. Rogalski
Institute of Applied Physics, Military University of Technology,
2 Kaliskiego Str., 00-908 Warsaw, Poland
e-mail: pmartyniuk@wat.edu.pl

GR contribution may be successfully limited by the barrier's incorporation to the detectors structure, while Auger GR mechanism could be suppressed either by the non-equilibrium conditions or designing the detectors with materials exhibiting lower Auger GR rates (Ashley and Elliott 1985; Maimon and Wicks 2006). The nBn architecture has been successfully implemented into $A^{III}B^{V}$ bulk compounds and InAs/GaSb type-II superlatices (T2SLs). The InAs/GaSb T2SLs success has resulted from the physical properties of the "artificial" material and what is most important, the zero valence band offsets with advantageous band alignment slightly harder to attain in $A^{III}B^{V}$ and $A^{II}B^{VI}$ bulk compounds (Ting et al. 2010). Although, T2SLs are considered to have advantage over bulk materials, there are indicators that, similarly to the technological problems related to the growth of self-organized quantum dot infrared detectors, T2SLs' InAs/GaSb development is limited by technological issues related to the growth of uniform and thick enough SLs (Martyniuk and Rogalski 2008). Moreover, short carrier lifetimes ($<$ 10 ns for $T > 200$ K) may hamper the development of the T2SLs IR devices (Wróbel et al. 2012).

The nBn architecture was also implemented into HgCdTe alloy exhibiting type-I heterojunction where theoretical modeling indicates a potential advantages in order to circumvent p-type doping in Molecular Beam Epitaxy (MBE) growth (Itsuno et al. 2011, 2012; Martyniuk and Rogalski 2013b).

Due to a nearly zero band valence offset with respect to AlAsSb in the valence band, InAsSb has emerged to play a dominant role in the designing of the nBn detectors (Klipstein 2008; Klem et al. 2010). Although theoretical prediction places T2SLs in front of the IR systems' development, the better stability over large area, higher carrier mobility and developed technology favours InAsSb in MWIR range (Vincent et al. 1990; Klipstein et al. 2011; Plis et al. 2011; Weiss et al. 2012).

In this paper we performed the detailed analysis of the InAsSb/AlAsSb nBn detector performance versus bias, operating temperatures, and structural parameters pointing out the HOT detector's optimal working conditions. Finally, the InAsSb/AlAsSb performance is compared to MCT "Rule 07".

2 Simulation procedure

The drift-diffusion (DD) model developed by Crosslight Software Inc. was used to simulate nBn InAsSb/AlAsSb detector. The material parameters are listed in Table 1. The electron affinity of both barrier layer (BL) and absorber layer (AL) are considered to be the most critical parameter to choose in nBn structure modeling. The valence band offset (VBO) varies from 80 to 270 meV for unbiased $InAs_{1-x}Sb_x/AlAs_{1-y}Sb_y$ structure ($x \approx y \approx 0.09$) at $T = 300$ K (Vurgaftman et al. 2001). The AlAsSb electron affinity was calculated using following dependence:

$$\gamma_y = 3.65 - 0.15y, \quad (1)$$

while the InAsSb's electron affinity was calculated according to the relation:

$$\gamma_x = A - 0.31x, \quad (2)$$

with $A = 5.72$, similarly to the relation given by IOFFE Physical Technical Institute. The simulations include radiative (RAD), SRH GR and both tunneling mechanisms at barrier-absorber (BL-AL) heterojunction. Since the AlAsSb's barrier height was estimated to be in range of ~2 eV, the GR mechanism in the BL is found to be negligible in assessing the bariode performance. In order to distinguish the intrinsic nBn performance, the n^+-type contact layer

Table 1 Parameters taken in modeling of MWIR InAsSb/AlAsSb nBn detectors

	Contact layer (CL)	Barrier layer (BL)	Absorber layer (AL)	Contact layer (CL)
Doping, $N_D\,(\text{cm}^{-3})$	10^{15}	10^{16}	$10^{14} \rightarrow 10^{17}$	$10^{14} \rightarrow 5 \times 10^{17}$
Doping Gauss tail, dx (μm)	0.05	0.05	0.05	0.02
Composition, x, y	0.09	0.08	$0.01 \rightarrow 0.36$	$0.01 \rightarrow 0.36$
Geometry, $d\,(\mu\text{m})$	0.25	0.3	1.5; 3	0.1
Electrical area, $A\,(\mu\text{m}^2)$		200×200		
Overlap matrix, F_1F_2	0.3	Auger coefficients: $C_n = 10^{-35}\text{cm}^6/\text{s}$, $C_p = 10^{-35}\text{cm}^6/\text{s}$	0.3	0.3
Trap energy level, E_{Trap}	$0.25E_g$	$0.5E_g$	$0.25E_g$	$0.25E_g$
Trap concentration, $N_{Trap}\,(\text{cm}^{-3})$	10^9	10^4	10^9	10^9
Minority carrier lifetime SHR/TAT, τ_n, $\tau_p\,(\mu\text{s})$	50; 0.5	50; 0.5	50; 0.5	50; 0.5
Incident power density, $\Phi_B\,(\text{W/cm}^2)$			0.05	

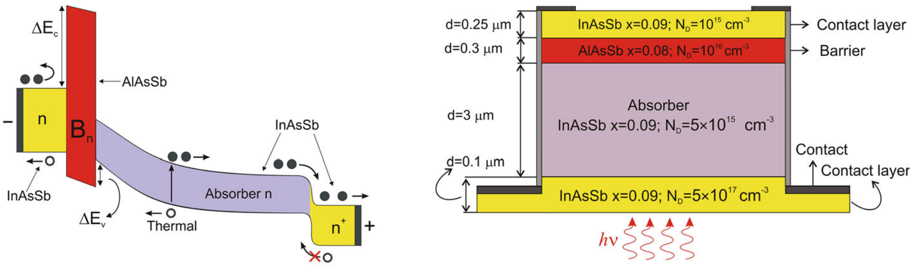

(a) **(b)**

Fig. 1 **a** Energy band diagram of the simulated nBn photodetector under reverse bias conditions. **b** The modelled nBn InAsSb/AlAsSb structure (Martyniuk and Rogalski 2013c)

(CL) is incorporated to eliminate the holes' generation contribution to the DD model at the n^+ region (see Fig. 1a, b). The detailed description of the growth procedure and device's characterization could be found in the papers by (Klipstein et al. 2011) and (Weiss et al. 2012).

The noise current is calculated using the expression including thermal Johnson-Nyquist noise and electrical shot noise:

$$i_n\,(V) = \sqrt{4k_BT/RA + 2qJ_{DARK}}, \tag{3}$$

where: A is a detector's area and k_B is the Boltzmann constant.

The quantum efficiency is a function of the incident radiation wavelength and current responsivity, R_i, according to the relation (without electro-optical gain):

$$\eta\,(\lambda) = 1.24\frac{R_i}{\lambda}. \tag{4}$$

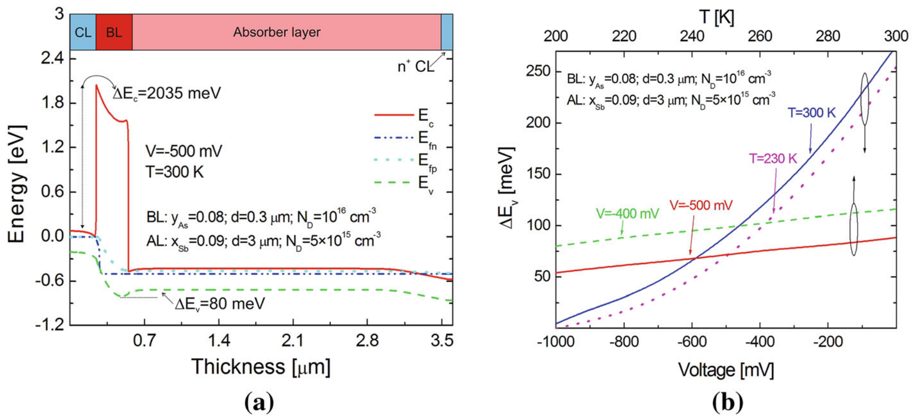

Fig. 2 **a** Calculated energy band diagram for the nBn InAsSb/AlAsSb for $V = -500\,\mathrm{mV}$. **b** $\varDelta E_v$ for BL-AL interface versus applied voltage and temperature

The detector's detectivity is defined by the expression:

$$D^* = \frac{R_i}{i_n\left(V\right)}\sqrt{A}. \tag{5}$$

3 nBn InAsSb/AlAsSb band alignment

The calculated energy band diagram for biased conditions ($V = -500\,\mathrm{mV}$) is depicted in Fig. 2a. The InAsSb/AlAsSb system exhibits "staggered" type-II heterojunction, where VBO could be controlled by proper BL/AL compositions and doping levels. The nBn detector requires "turn-on" voltage to align the valence band (at BL-AL interface) allowing nearly unimpeded minority carrier transport to CL. It was estimated that applying $V = -500\,\mathrm{mV}$, the energy barrier for holes is being reduced to $\sim$80 meV in comparison with the equilibrium conditions.

Figure 2b presents $\varDelta E_v$ (refer to Fig. 1a) versus voltage and operating temperature. The minority carriers in bariode are efficiently blocked for the $\varDelta E_v > 3k_BT$. The applied voltage mostly influences $\varDelta E_v$, while $\varDelta E_c$ keeps nearly constant. It was found that for the BL-AL interface $\varDelta E_v \approx 270 \rightarrow 4\,\mathrm{meV}$ and for the CL-BL interface $\varDelta E_c \approx 2032 \rightarrow 2038\,\mathrm{meV}$ for $V = 0 \rightarrow 1\mathrm{V}$, respectively. The condition of unimpeded minority carrier transport to the CL ($\varDelta E_v < 3k_BT = 78\,\mathrm{meV}$ at $T = 300\,\mathrm{K}$) is met for $V > -500\,\mathrm{mV}$. $\varDelta E_v$ slightly increases with temperature (see Fig. 2b) while $\varDelta E_c$ should be barely influenced by T.

4 Dark and photocurrent modeling

The nBn detector operates in minority carrier manner. Dark current is driven mainly due to the hole transport from AL to CL. Figure 3a shows calculated dark current characteristics versus temperature for both nBn and p$^+$-on-n InAsSb ($x = 0.09$) photodiode for two selected voltages (-300 and $-500\,\mathrm{mV}$). In analyzed temperature range, nBn detector is diffusion limited exhibiting characteristic one slope behaviour. The simulation results were compared to experimental ones (for $V = -400\,\mathrm{mV}$) which could be fitted by the

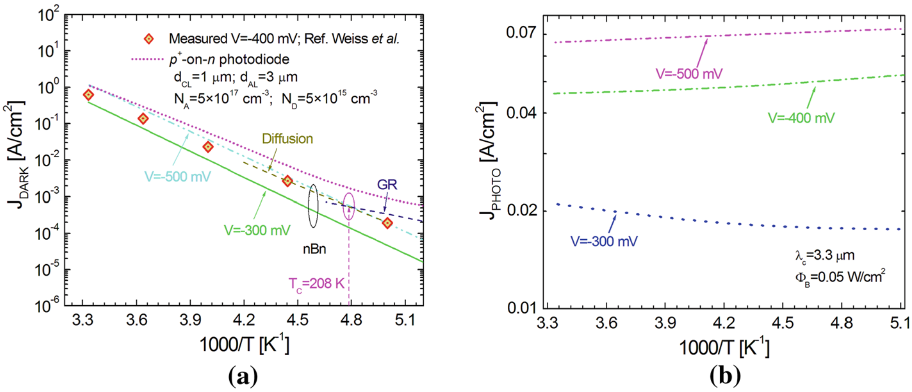

Fig. 3 **a** J_{DARK} versus reciprocal temperature for selected voltages. **b** J_{PHOTO} versus reciprocal temperature for selected voltages for InAsSb/AlAsSb nBn detector. The experimental results are taken after (Weiss et al. 2012)

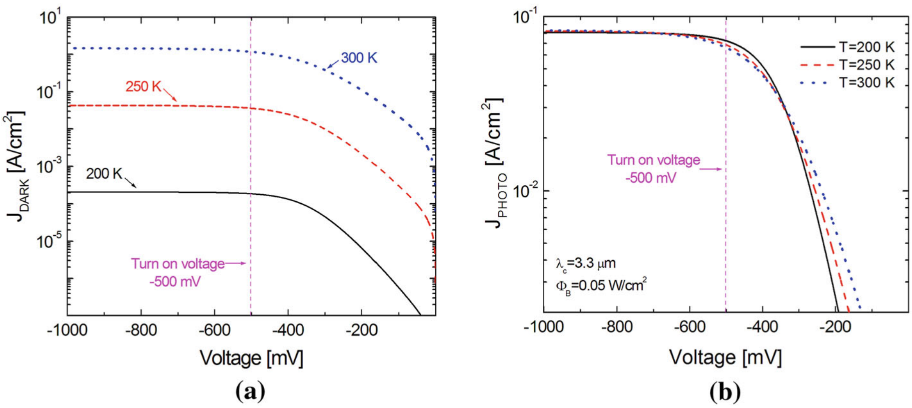

Fig. 4 **a** J_{DARK} versus voltage for selected temperatures. **b** J_{PHOTO} versus voltage for selected temperature for InAsSb/AlAsSb nBn detector

relation: $\propto T^3 exp\,(-0.34q/k_BT)$, where 0.34 eV represents the AL's band-gap energy at $T = 0$ K. The depletion region in p^+-on-n photodiode, leads to the characteristic two slope behaviour, where the GR contribution could be expressed by the similar formula assuming $\propto T^{1.5} exp\,(-0.17q/k_BT)$; where 0.17 eV represents $E_{Diff}/2(E_{Diff} = 0.34\,\text{eV})$. The GR contribution to the net J_{DARK} in photodiode dominates below $T_C = 208$ K (crossover temperature) while above the diffusion contribution plays decisive role. Comparing dark currents of the nBn and p^+-on-n photodiode having the same AL's doping indicates that bariode may surpass photodiode's performance close to the crossover temperature ($T_C = 208$ K) while at room temperature the performance of both type of detectors is comparable due to the fact that devices are diffusion limited.

The temperature dependence of photocurrent, exhibits different features within three voltage regions presented in Figs. 3b and 4b. J_{PHOTO} was calculated for $\lambda = 3.3\,\mu$m and incident power density $\Phi_B = 0.05\,\text{W/cm}^2$. For biases to -300 mV, J_{PHOTO} increases for T being within the range of 200–300 K. In the bias range $-300\,\text{m}V < V < -600$ mV the opposite dependence is observed, while for $V > -600$ mV again J_{PHOTO} raises with T. This behav-

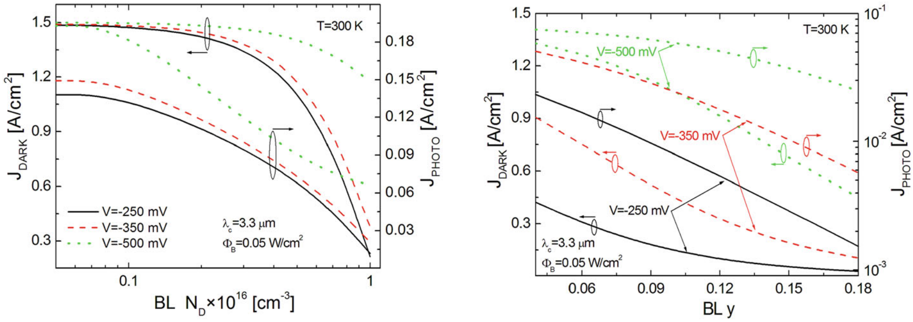

(a) **(b)**

Fig. 5 **a** J_{DARK} and J_{PHOTO} versus BL's doping. **b** J_{DARK} and J_{PHOTO} versus BL's composition for InAsSb/AlAsSb nBn detector

iour may be attributed to the fact that AL band-gap energy decreases from 311 to 286 meV in temperature range 200–300 K which effectively increase $\Delta E_v (\Delta E_v = 80 - 110$ meV for $T =$ 200–300 K). The both InAsSb and AlAsSb electron affinities were assumed to be dependent on alloy composition.

The influence of ΔE_v-barrier is clearly evident in Fig. 4a, b, which present calculated J_{DARK} and J_{PHOTO} voltage characteristics. The "turn-on" voltage was estimated to be $V = -500$ mV for both J_{DARK} and J_{PHOTO}. In considered temperature range, three distinct regions in J_{DARK} voltage characteristics may be distinguished. For biases between 0 and -50 mV, J_{DARK} is sensitive to bias while in the bias range from -50 to -500 mV, J_{DARK} is less voltage dependent in comparison with low voltage. This behaviour could be explained by the fact that ΔE_v for $V = -500$ mV is comparable with $3k_BT$ which means that minority carriers are nearly freely transported to the CL giving contribution to the net J_{DARK}. It was shown, that for voltages $V < -500$ mV, the dark current increases sharply, while above $V > -500$ mV, the dark current saturates. J_{PHOTO} exhibits the same trend as J_{DARK} keeping almost constant above $V > -500$ mV, while for the low biases only one distinct region could be discriminated where J_{PHOTO} is bias sensitive.

The choice of the BL's doping and composition plays crucial role in designing nBn structures. Optimization should be performed for the chosen voltage due to the fact that both ΔE_v and ΔE_c depend on applied bias. Once BL doping increases, the ΔE_c slightly raises while ΔE_v drops. For barrier's doping $N_D < 2 \times 10^{15}$cm^{-3}, the dark current does not exhibit doping and voltage dependence (see Fig. 5a), while above $N_D > 2 \times 10^{15}$ cm^{-3} J_{DARK} decreases which could be attributed to ΔE_c raising with doping and this effect is much more visible for lower voltages where minority carrier's transport to the CL is more impeded.

Similar considerations are conducted for barrier's composition (see Fig. 5b). Direct dependence of the ΔE_c and ΔE_v on composition and voltage is responsible for the both dark and photocurrent characteristics. Once BL's composition increases, both J_{DARK} and J_{PHOTO} decrease. The cap layer's doping and composition also influence the performance of nBn detectors. Again CL's doping optimization should be performed for given bias. The J_{DARK} and J_{PHOTO} dependence on CL's doping, N_D, is more evident for lower voltages (see Fig. 6a). Above turn on voltage both J_{DARK} and J_{PHOTO} keep nearly constant in analyzed doping range. The composition of CL seems not to have visible influence on J_{PHOTO} and J_{DARK} which is presented in Fig. 6b.

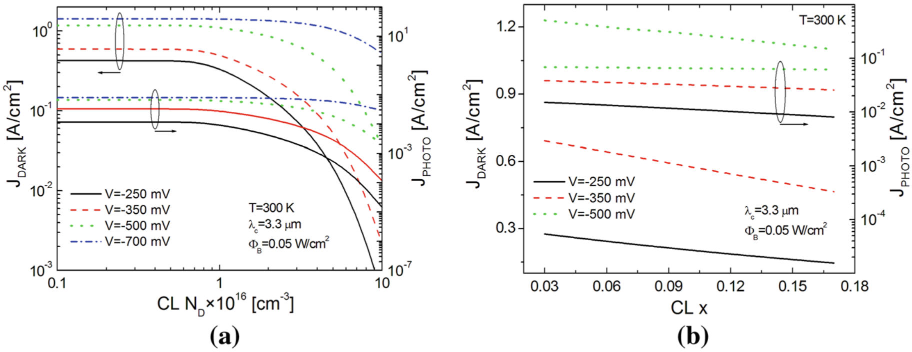

Fig. 6 **a** J_{DARK} and J_{PHOTO} versus CL's doping. **b** J_{DARK} and J_{PHOTO} versus CL's composition for InAsSb/AlAsSb nBn detector

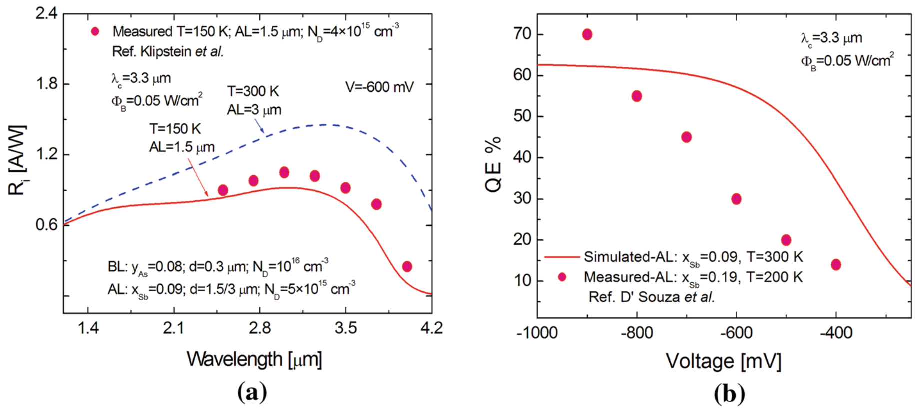

Fig. 7 **a** Spectral current responsivity for selected AL's thicknesses. **b** QE versus applied voltage for InAsSb/AlAsSb nBn detector. The experimental results are taken after (Klipstein et al. 2011; D' Souza et al. 2012)

5 Quantum efficiency and responsivity

The spectral current responsivity (R_i) versus wavelength is calculated for two AL's widths (1.5 and 3 μm) and two operating temperatures ($T = 150$ and 300 K) for bias voltage $V = -600$ mV to reach the highest QE in the range close to 60 %. The experimental results are presented for structure with AL's doping of $N_D = 4 \times 10^{16}$ cm^{-3} and thickness of 1.5 μm The proper agreement between theoretical prediction and experimental results are obtained (Klipstein et al. 2011). The maxiumu R_i is reached for $\lambda = 3.3$ μm while 50 % cut off wavelength (λ_c) is found to be 4.2 μm at $T = 300$ K (see Fig. 7a). The ΔE_v directly affects the QE which in turn influences J_{PHOTO}. The QE dependence on voltage is depicted in Fig. 7b. Once reverse voltage increases, QE raises sharply to the value of 60 % at $V = -600$ mV. Above this bias, the QE is not practically influenced by the VBO, reaching the value in the range of ≈ 65 %. Comparing the $J_{DARK}(V)$ and $J_{PHOTO}(V)$ curves presented in Figs. 3a and 4b, it is clearly visible that nBn structures may be biased above $V > -600$ mV due to the fact that there is no tunneling contribution and J_{DARK} saturates, while QE reaches its maximum value.

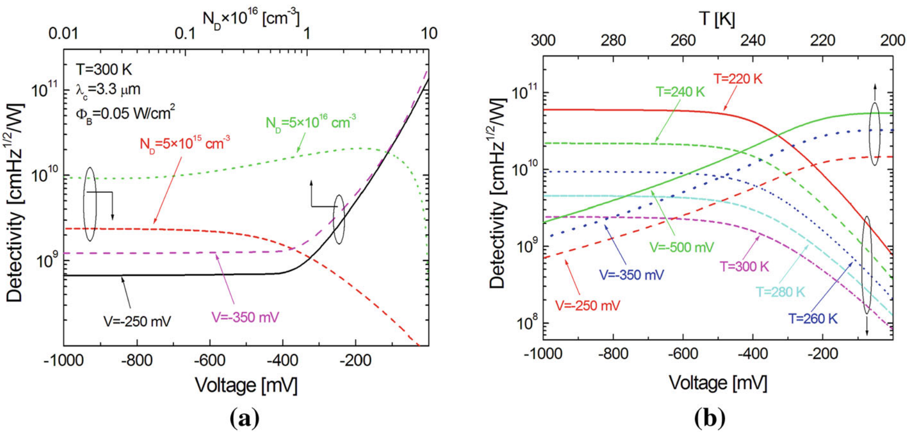

Fig. 8 **a** Detectivity versus applied voltages and AL's doping. **b** Detectivity versus voltage and temperature for InAsSb/AlAsSb nBn detector

6 Detectivity

The detectivity of detectors operating at room temperature is limited by electrical shot noise, that is why the background induced shot noise was not included in modeling. The D^* versus bias voltage and AL's doping is presented in Fig. 8a.

The simulation results point out that for considered structure (AL's $N_D = 5 \times 10^{15}\,\mathrm{cm}^{-3}$; BL's $N_D = 10^{16}\,\mathrm{cm}^{-3}$), the estimated maximum detectivity is in the range of $\sim 3 \times 10^9\,\mathrm{cmHz}^{1/2}$/W. D^* versus applied voltage tends to saturate for $V > -500\,\mathrm{mV}$, while below this value the detectivity is mostly influenced by the ΔE_v-barrier limiting transport of the photogenerated carriers (low *QE*, see Fig. 7b).

The unfavourable conditions related to the VBO could be circumvented by the proper choice of AL's doping (in comparison with the BL layer doping, $N_D = 10^{16}\,\mathrm{cm}^{-3}$), which effectively reduces the ΔE_v in low voltage range. In comparison with the AL's doping in the level of $5 \times 10^{15}\,\mathrm{cm}^{-3}$, the maximum of $D^* = 2 \times 10^{10}\,\mathrm{cmHz}^{1/2}$/W may be reached for $V = -150\,\mathrm{mV}$ and $N_D = 5 \times 10^{16}\,\mathrm{cm}^{-3}$ (Martyniuk and Rogalski 2013c). Further increase of the bias voltage causes rapid increase of the dark current which results in lowering detectivity below $10^{10}\,\mathrm{cmHz}^{1/2}$/W. The both AL's and BL's optimal doping are directly related to each other, which is reflected by the D^* dependence on the AL's doping (see Fig. 8a). For analyzed voltages (-250, $-350\,\mathrm{mV}$) the detectivity keeps constant in the range of $\approx (0.7 - 1.1) \times 10^9\,\mathrm{cmHz}^{1/2}$/W for the AL's doping in the range of $10^{14} \rightarrow 10^{16}\,\mathrm{cm}^{-3}$, while above doping of $10^{16}\,\mathrm{cm}^{-3}$, the rapid increase of the D^* is observed (BL's doping, $N_D = 10^{16}\,\mathrm{cm}^{-3}$). The detectivity dependence on operating temperature is presented in Fig. 8b. We can see that detectivity close to $10^{11}\,\mathrm{cmHz}^{1/2}$/W can be achieved in operating temperature easily reached by thermoelectrical coolers ($T = 220\,\mathrm{K}$).

The detectivity of nBn structures highly depends on both BL and CL's doping which is presented in Fig. 9a, b, respectively. For assumed AL doping ($N_D = 5 \times 10^{15}\,\mathrm{cm}^{-3}$) and CL doping ($N_D = 10^{15}\,\mathrm{cm}^{-3}$) the highest D^* may be reached for BL doping of $N_D < 6 \times 10^{15}\,\mathrm{cm}^{-3}$, while above this doping level the detectivity drops sharply due to the fact that ΔE_v increases with BL's doping (see Fig. 9a). Assuming BL's doping of $N_D = 10^{16}\,\mathrm{cm}^{-3}$, the maximum D^* could be reached for CL doping of $N_D < 2 \times 10^{16}\,\mathrm{cm}^{-3}$ depending on

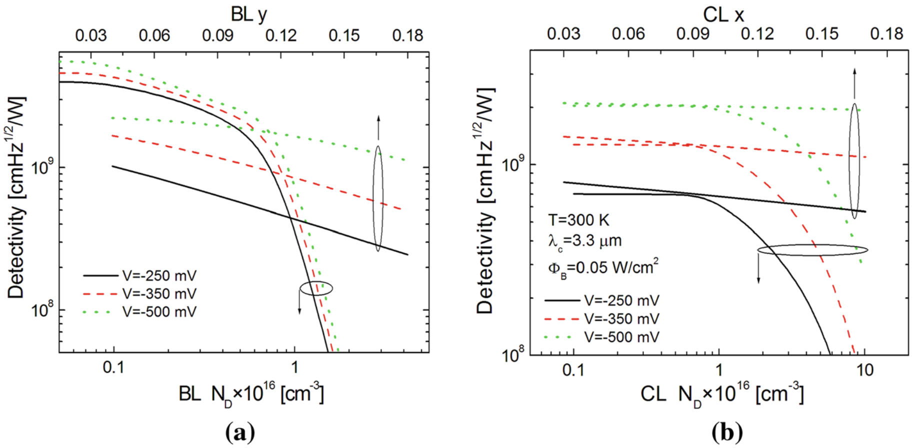

Fig. 9 **a** Detectivity versus BL's doping and composition. **b** Detectivity versus CL's doping and composition for InAsSb/AlAsSb nBn detector

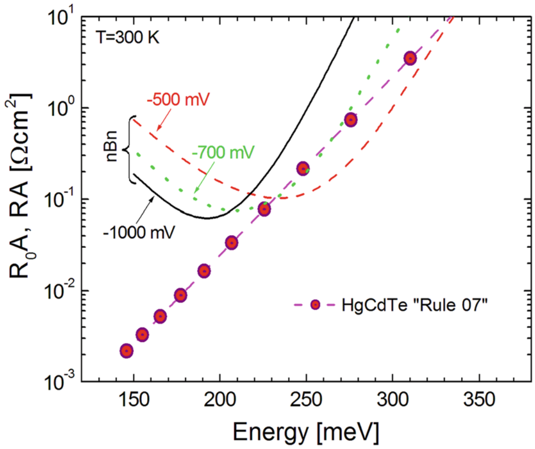

Fig. 10 *RA* product of MWIR nBn InAsSb/AlAsSb versus AL band-gap energy. R_0A calculated in accordance with MCT "Rule 07"

applied bias. Once BL's and CL's composition increases, the detectivity decreases. The BL's composition influences D^* much more in comparison with CL's composition.

7 Comparison of the IR technologies

Figure 10 shows the dependence of the *RA* product on the AL's band gap energy at room temperature for InAsSb/AlAsSb nBn. Similarly to Ting *et al.* the InAsSb nBn *RA* is compared to the MCT "Rule 07" being an effective mean of evaluating of IR detectors (Tennant et al. 2008; Ting et al. 2010) in order to point out the current status of the InAsSb/AlAsSb technology. It is visible that InAsSb/AlAsSb nBn structures exhibit *RA* value comparable or higher in comparison with the best R_0A product of HgCdTe photodiodes with the same AL's bandgap. Figure 11 presents *RA* product of the nBn structures versus bias voltage for selected AL's InAsSb composition. The presented results indicate that nBn structures require proper biasing to reach high *QE* and *RA* product. It must be stressed that in low voltage region the nBn

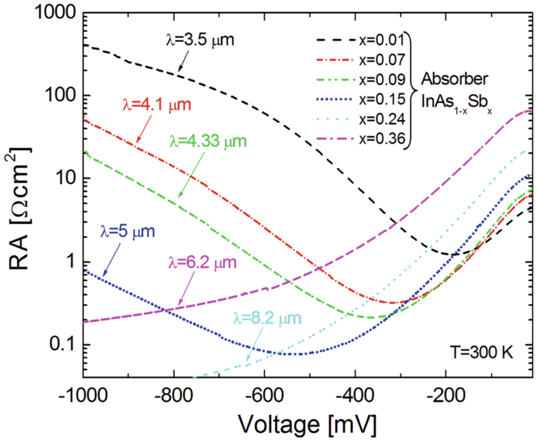

Fig. 11 *RA* product versus voltage of MWIR nBn InAsSb/AlAsSb structure for selected AL's composition

performance is limited by low *QE*. The InAsSb/AlAsSb nBn goes to BLIP condition around $T \approx 185\,\text{K}$ ($x = 0.09$).

8 Conclusion

The performance of MWIR InAsSb/AlAsSb nBn detectors for HOT temperature operation has been analyzed. In order to reach the high *QE*, the proper VBO is essential which could be met by suitable biasing; AL, BL and CL's compatibility in terms of composition and doping.

The theoretically predicted results are compared with experimental data showing appropriate level of agreement in assumed operating conditions. The diffusion-GR behaviour crossover temperature was estimated pointing out that InAsSb/AlAsSb nBn detectors have a potential to surpass standard p^+-on-n photodiodes below T_C while at room temperature conditions, both technologies reach comparable J_{DARK}. In addition, at $T = 300\,\text{K}$ operation the nBn detectors allows to reach higher *RA* product for analyzed Sb's compositions (assuming BL $y = 0.08$) and voltages $V > -500\,\text{mV}$ in comparison with the trend line represented by MCT "Rue 07".

Acknowledgments We acknowledge support by National Centre of Research and Development-the grant no. PBS 1/B5/2/2012 and Polish Ministry of Sciences and Higher Education, Key Project POIG.01.03.01-14-016/08 "New Photonic Materials and their Advanced Application".

References

Ashley, T., Elliott, C.T.: Nonequlibrium devices for infra-red detection. Electron. Lett. **21**, 451–452 (1985)

D' Souza, A.I., Robinson, E., Ionescu, A.C., Okerlund, D., De Lyon, T.J., Sharifi, H., Roebuck, M., Yap, D., Rajavel, R.D., Dhar, N., Wijewarnasuriya, P.S., Grein, C.: Electroptical characterization of MWIR InAsSb detectors. J. Electron. Mater **41**, 2671–2678 (2012)

Itsuno, A.M., Philips, J.D., Velicu, S.: Design and modeling of HgCdTe nBn detectors. J. Electron. Mater. **40**, 1624–1629 (2011)

Itsuno, A.M., Phillips, J.D., Velicu, S.: Mid-wave infrared HgCdTe nBn photodetector. Appl. Phys. Lett. **100**, 161102 (2012)
Klem, J.F., Kim, J.K., Cich, M.J., Hawkins, S.D., Fortune, T.R., Rienstra, J.L.: Comparison of nBn and nBp mid-wave barrier infrared photodetectors. Proc. SPIE. **7608**, 76081P (2010)
Klipstein, P.: XBn' barrier photodetectors for high sensitivity and high operating temperature infrared sensors. In: Proceedings of SPIE. 6940, 69402U–1-11 (2008)
Klipstein, P., Klin, O., Grossmann, S., Snapi, N., Yaakobovitz, B., Brumer, M., Lukomsky, I., Aronov, D., Yassen, M., Yofis, B., Glozman, A., Fishman, T., Berkowitz, E., Maen, O., Shtrichman, I., Weiss, E.: MWIR InAsSb XBn detector for high operating temperatures. Proc. SPIE **8012**, 80122R (2011)
Maimon, S., Wicks, G.: nBn detector, an infrared detector with reduced dark current and higher operating temperature. Appl. Phys. Lett. **89**, 151109–1-3 (2006)
Martyniuk, P., Rogalski, A.: Comparison of performance of quantum dot and other types infrared photodetectors. Proc. SPIE **6940**, 694004 (2008)
Martyniuk, P., Rogalski, A.: Modeling of MWIR HgCdTe complementary barrier HOT detector. Solid State Electron. **80**, 96–104 (2013b)
Martyniuk, P., Rogalski, A.: HOT infrared detectors. Opto-Electron. Rev. **21**, 239–257 (2013a)
Maryniuk, P., Rogalski, A.: Modeling of InAsSb/AlAsSb nBn HOT detector's performance limit. In: Proceedings of SPIE 8704–55 (2013c)
Plis, E., Myers, S., Kutty, M.N., Mailfert, J., Smith, E.P., Johnson, S., Krishna, S.: Lateral diffusion of minority carriers in InAsSb-based nBn detectors. Proc. SPIE **7945**, 79451R (2011)
Rogalski, A.: Infrared Detectors, 2nd edn. CRC Press, Boca Raton (2011)
Tennant, W.E., Lee, D., Zandian, M., PiQuette, E., Carmody, M.: MBE HgCdTe technology: a very general solution to IR detection, described by, Rule07", a very convenient heuristic. J. Electron. Mater. **37**, 1406–1410 (2008)
Ting, D.Z., Hill, C.J., Soibel, A., Nguyen, J., Keo, S., Lee, M.C., Mumolo, J.M., Liu, J.K., Gunapala, S.D.: Antimonide-based barrier infrared detectors. Proc. SPIE **7660**, 76601R (2010)
Vincent, W., Chin, L., Egan, R.J., Tansley, T.L.: Electron mobility in $InAs_{1-x}Sb_x$ and the effect of alloy scattering. J. Appl. Phys. **69**, 6 (1990)
Vurgaftman, I., Meyer, J.R., Ram-Mohan, L.R.: Band parameters for III–V compound semiconductors and their alloys. J. Appl. Phys. **89**, 5815 (2001)
Weiss, E., Klin, O., Grossmann, S., Snapi, N., Lukomsky, I., Aronov, D., Yassen, M., Berkowitz, E., Glozman, A., Klipstein, P., Freankel, A., Shtrichman, I.: InAsSb-based XB_nn bariodes grown by molecular beam epitaxy on GaAs. J. Cryst. Growth **339**, 31–35 (2012)
Wróbel, J., Martyniuk, P., Plis, E., Madejczyk, P., Gawron, W., Krishna, S., Rogalski, A.: Dark current modeling of MWIR type-II superlattice detectors. Proc. SPIE **8353**, 8353–16 (2012)